Estimating the noise level function with the tree of shapes and non-parametric statistics

Baptiste Esteban, Guillaume Tochon, and Thierry Géraud

EPITA Research and Development Laboratory (LRDE), Le Kremlin-Bicêtre, France
{baptiste.esteban, guillaume.tochon, thierry.geraud}@lrde.epita.fr

Abstract. The knowledge of the noise level within an image is a valuable information for many image processing applications. Estimating the noise level function (NLF) requires the identification of homogeneous regions, upon which the noise parameters are computed. Sutour *et al.* have proposed a method to estimate this NLF based on the search for homogeneous regions of square shape. We generalize this method to the search for homogeneous regions with arbitrary shape thanks to the tree of shapes representation of the image under study, thus allowing a more robust and precise estimation of the noise level function.

Keywords: Noise level function· Tree of shapes· Non-parametric rank correlation.

1 Introduction

Natural images are inherently corrupted by digital noise resulting from the various imperfections occuring during the acquisition chain (such as sensor noise, quantization noise, and so on). Efficiently handling or removing the noise is a fundamental task in image processing, but it requires a precise knowledge of the noise attributes. By providing the relationship between the intensity of the image pixels and the noise variance, the noise level function [16] (NLF) is a valuable information to estimate, not only for image denoising purposes [3], but also for image segmentation [11], image compression [23] or super-resolution [12]. When the noise is signal-independent, classical separation approaches can be applied to estimate its properties [10,17]. For signal-dependent noise (such as Poisson and Poisson-Gaussian), variance stabilization techniques have first to be applied [18,21], but their optimal use requires a certain knowledge of the noise, leading to a chicken-and-egg situation. As an alternative to separation techniques, Beaurepaire *et al.* [2] proposed to first identify some homogeneous regions in the image, on which the noise parameters can be further evaluated. In order to be independent of the noise statistical distribution, Sutour *et al.* [22] proposed a non-parametric method to detect these homogeneous areas. However, their definition as square blocks does not facilitate their detection, as their shape makes them unsuited to the image content. The use of patches adapting locally to the image morphological content would allow a better identification of these homogeneous regions, and therefore yield a more robust estimation of the NLF.

This idea of adaptive patches has already been investigated in the literature for image denoising purposes [9,8], but to the best of our knowledge, it has never been implemented to estimate the NLF.
In this article, we extend the NLF estimation method developed by Sutour *et al.* [22]. More specifically, we no longer seek for square homogeneous blocks, but we rather search for arbitrarily shaped homogeneous regions based on the tree of shapes (ToS) [19,1] representation of the considered image. This hierarchical representation naturally provides areas whose contours follow the level lines of the image (seen as a topographic map), thus adapted to its morphological content. We show that the extraction of the most relevant shapes from the ToS allows to obtain a more robust NLF estimation than in the case of square blocks.
The present article is organized as follows: Section 2 summarizes the method proposed by Sutour *et al.* [22]. In Section 3, we introduce our generalized search for homogeneous regions of arbitrary shapes, based on a Mumford-Shah simplification of the ToS representation. Qualitative and quantitative comparisons between the method proposed by Sutour *et al.* [22] and ours are presented in Section 4, while Section 5 concludes and draws some perspectives of our work.

2 NLF estimation with square blocks

The NLF estimation proposed by Sutour *et al.* [22] is decomposed in two steps:

1. the detection of homogeneous square blocks through a non-parametric statistical test based on Kendall τ rank correlation coefficient,
2. the identification of the NLF, *i.e.* the relation linking the intensity of the image pixels to the noise variance.

In the following, $f : \Omega \subset \mathbb{Z}^2 \to \mathbb{R}$ will denote an image that associates a numeric value $x_i = f(i)$ to any pixel $i \in \Omega$.

2.1 The Kendall τ coefficient

The i^{th} block of pixels $b_i \subset \Omega$ is said to be homogeneous if its pixel values fluctuate only because of the noise, and not because of the image content. In order not to depend on any assumption on the nature of the noise, the homogeneous block detection step is formulated as a non-parametric hypothesis test using the Kendall τ rank correlation coefficient [15]. Let $x \in \mathbb{R}^n$ and $y \in \mathbb{R}^n$ be two sequences of n observations of two random variables X and Y. The Kendall τ coefficient $\tau(x, y)$ is defined on the interval $[-1, 1]$ by :

$$\tau(x,y) \;=\; \frac{1}{n(n-1)} \sum_{1 \le i,j \le n} \operatorname{sign}(x_i - x_j)\, \operatorname{sign}(y_i - y_j), \tag{1}$$

with $x_i \neq x_j$ and $y_i \neq y_j$, $\forall i \neq j$.
In the associated statistical test, $\tau(x, y) = 0$ constitutes the null hypothesis H_0 and indicates an absence of correlation between the values of x and y. Equation (1)

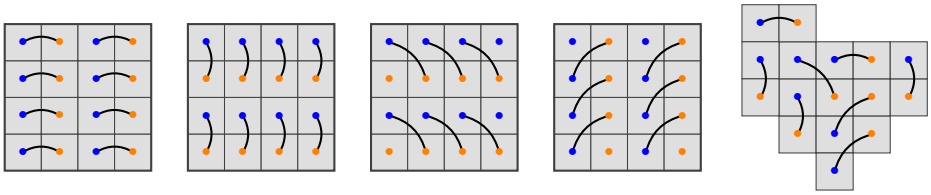

Fig. 1. First four cases: the tested region has a square shape, its pixel values are divided in sequences x and y following the horizontal, vertical, diagonal, and anti-diagonal relationships. When the tested region is extracted from the ToS and has an arbitrary shape (rightmost case), the splitting in sequences x and y is performed randomly.

can be reformulated to take into account any tied pairs (if $x_i = x_j$ or $y_i = y_j$) [14]. Under H_0 (absence of correlation between X and Y), the z-score associated with $\tau(x, y)$ follows a standard normal distribution $\mathcal{N}(0, 1)$ [22, Proposition 3.6]. Conversely, the alternative hypothesis H_1 is declared when $\tau(x, y) \neq 0$, that is, when the fluctuation of the pixel values in b_i cannot be explained by the noise only (because of the presence of an edge within the block for instance).

2.2 Detection of homogeneous blocks

In Sutour *et al.* [22], the studied image is divided in blocks b_i of size 16×16 pixels. The pixel values of each block b_i are split in two sequences x and y for which the Kendall τ coefficient $\tau(x, y)$ is computed. If the p-value $p = \mathbb{P}(\tau(X, Y) > \tau(x, y)|H_0)$ is greater than a predefined detection threshold α, the null hypothesis H_0 is accepted, meaning that the values of the two sequences x and y are uncorrelated. The block b_i is thus declared homogeneous.
In practice, b_i is split in $K = 4$ sequences $x^{(k)}$ and $y^{(k)}$ following the horizontal, vertical, diagonal and anti-diagonal neighborhood relationships, as displayed by Figure 1. b_i is then declared homogeneous if all K p-values p_k exceed the detection threshold:

$$\min_k \left\{ p_k \;=\; \mathbb{P}\left(\tau(X, Y) > \tau(x^{(k)}, y^{(k)}) \,|\, H_0\right) \right\} \;>\; \alpha. \tag{2}$$

2.3 NLF estimation

The NLF defines the relation between the intensity of the image pixels and the variance of the noise corrupting them. Sutour *et al.* [22] proposed a positively increasing second degree polynomial relation for the NLF: $\sigma_i^2 = \mathrm{NLF}_{(a,b,c)}(x_i) = ax_i^2 + bx_i + c$, with $(a, b, c) \in (\mathbb{R}^+)^3$. This notably allows to model the additive Gaussian noise (whose NLF $\sigma_i^2 = c$ is constant, hence $(a, b) = (0, 0)$), the Poisson noise (with linear NLF $\sigma_i^2 = bx_i$, thus $(a, c) = (0, 0)$), the multiplicative/Gamma noise (whose NLF $\sigma_i^2 = ax_i^2$ is parabolic, hence $(b, c) = (0, 0)$), and their different mixtures (such as the Poisson-Gaussian noise for instance).

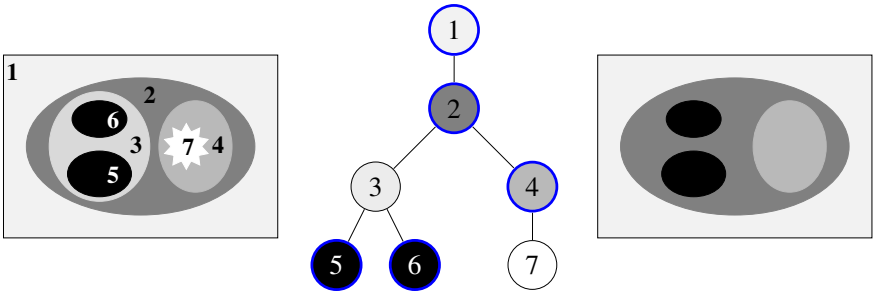

Fig. 2. Left: input image; Middle: corresponding tree of shapes; Right: Mumford-Shah simplification where the optimal partition is composed of the level lines of the nodes circled in blue.

First, the empirical mean $\hat{\mu}_i = \mathbb{E}[b_i]$ and empirical variance $\hat{\sigma}_i^2 = \mathrm{Var}[b_i]$ of each homogeneous block b_i are calculated. Following, the NLF coefficients are estimated as those minimizing the residual error between the empirical variance $\hat{\sigma}_i^2$ and the variance predicted by the NLF relation $\mathrm{NLF}_{(a,b,c)}(\hat{\mu}_i)$ for all homogeneous block b_i:

$$\widehat{(a,b,c)} = \underset{(a,b,c)\in(\mathbb{R}^+)^3}{\operatorname{argmin}} \sum_i \|\mathrm{NLF}_{(a,b,c)}(\hat{\mu}_i) - \hat{\sigma}_i^2\|_1. \tag{3}$$

Despite being more complex to solve than a L^2 minimization (which could be solved by classical least-square estimation), the L^1 minimization used in equation (3) is more robust to outliers and is solved in practice thanks to the preconditioned primal-dual Chambolle-Pock algorithm [6].

3 NLF estimation with the tree of shapes

The drawback of searching for homogeneous square blocks is that their shape is not adaped to the morphological content of the image. Thus, depending on the input image, it might be complicated to detect sufficiently enough of these blocks in order to get a robust and precise estimation of the NLF. Here, we relax the constraint on the shape of the sought homogeneous regions. For that purpose, we propose to use regions adapted to the image content, extracted from the ToS representation of the considered image.

3.1 The tree of shapes

The tree of shape (ToS) is a hierarchical structure belonging to the field of mathematical morphology [19]. For $\lambda \in \mathbb{R}$, we define the lower level set of f (of level λ) as $[f < \lambda] = \{i \in \Omega \mid f(i) < \lambda\}$ and the upper level set as $[f \geq \lambda] = \{i \in \Omega \mid f(i) \geq \lambda\}$. A *shape* $\mathcal{C} \subset \Omega$ is a connected component belonging to one of these two sets, with its holes filled [13]. The ToS $\mathcal{T}$ of an image encodes the inclusion relationship between the different shapes of the image in a

Fig. 3. Input noisy image (left) and examples of Mumford-Shah simplifications applied to its ToS with regularization parameter $\nu = 500$ (center) and $\nu = 2000$ (right).

hierarchical manner. The border $\partial\mathcal{C}_i$ of each shape $\mathcal{C}_i$ corresponds to a level line of the image (when seen as a topographic relief). The ToS therefore represents the inclusion of all level lines of the image, as displayed in Figure 2.
Note that the ToS can be computed very efficiently: an algorithm with a linear complexity with respect to the number of pixels exists [5], and it can be parallelized [7].

3.2 Mumford-Shah simplification of the tree of shape

After its construction, the ToS representation is composed of meaningful shapes (in terms of image content description), but it also contains small and/or meaningless shapes (notably the leaves and regions close to the root of the tree). Thus, prior to conducting the homogeneity test, a simplification of the ToS according to the Mumford-Shah functional is performed in order to filter out those meaningless shapes. This ToS simplification procedure is based on the Mumford-Shah image segmentation principle [20]. If $\pi = \bigsqcup_i R_i$ is a partition of Ω, and if $\bar{f}_i$ is the mean value of f on region $R_i \subset \Omega$, the (piecewise constant) Mumford-Shah functional of f on π is defined as

$$E_\nu(f,\pi) = \sum_{R_i \in \pi} \left(\iint_{R_i} (\bar{f}_i - f)^2 dxdy + \frac{\nu}{2}|\partial R_i| \right), \tag{4}$$

where $|\partial R_i|$ is the length of the border of R_i and ν is a regularization parameter of the functional. Finding the partition π that minimizes equation (4) without any further constraint on π remains an arduous and non-convex optimization task.
When this energy minimization procedure is subordinated to the ToS structure however, the region borders $\partial\mathcal{R}_i$ are fixed since they are defined as the contours $\partial\mathcal{C}_i$ of the shapes $\mathcal{C}_i \in \mathcal{T}$. It thus becomes possible to find the optimal segmentation with a greedy algorithm that iteratively removes shapes to decrease the energy functional (see [24] for more details). In practice, the Mumford-Shah simplification of $\mathcal{T}$ yields a simplified ToS $\mathcal{T}_\nu^\star$ where some initial shapes have been

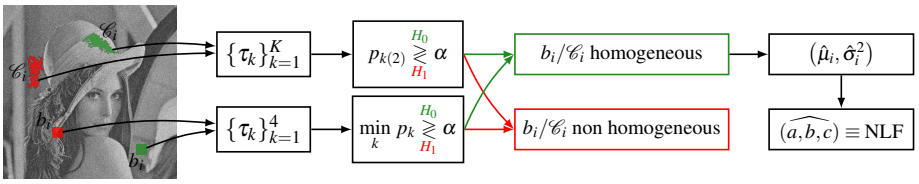

Fig. 4. Illustration of the stages for the NLF estimation from blocks b_i and from shapes $\mathcal{C}_i$.

filtered out, such that the segmentation $\partial\mathcal{T}_\nu^\star$ formed by the union of the level lines of the remaining shapes in $\mathcal{T}^\star$ minimizes the Mumford-Shah functional (4) for a given value of the regularization parameter:

$$\mathcal{T}_\nu^\star = \underset{\mathcal{T}_\nu'}{\operatorname{argmin}}\ E_\nu\left(f, \partial\mathcal{T}_\nu'\right), \tag{5}$$

where $\mathcal{T}_\nu'$ is a simplified ToS with some shapes of $\mathcal{T}$ have been removed, and $\partial\mathcal{T}_\nu'$ is the partition of Ω that is obtained by taking the union of the level lines of all shapes in $\mathcal{T}_\nu'$. An example of Mumford-Shah simplification is presented in Figure 2, where the shapes $\mathcal{C}_3$ and $\mathcal{C}_7$ have been filtered out from the orignal ToS, leading to the rightmost partition obtained as the union of the level lines of the remaining shapes (circled in blue).

3.3 Detection of homogeneous shapes

The ToS representation of the noisy input image f is composed of shapes with very irregular contours, and with a limited depth of inclusion. Thus, we first smooth f with a Gaussian filter prior to the construction of its ToS. This yields an increased number of shapes with regularized contours, and a greater depth of inclusion in the ToS.

The obtained ToS is simplified according to the Mumford-Shah functional for several values of the regularization parameter ν, yielding several simplified ToS $\mathcal{T}_\nu^\star$ whose shapes are pooled together in a set of candidate shapes $\mathcal{C}^\cup = \bigcup_\nu \{\mathcal{C} \in \mathcal{T}_\nu^\star\}$ of various sizes and complexities, as illustrated in Figure 3.

The homogeneity test is then conducted on all candidate shapes $\mathcal{C}_i \in \mathcal{C}^\cup$ with the pixel values of the noisy image $f(\mathcal{C}_i)$ and not those of the filtered image. In order to compute the Kendall $\tau(x, y)$ coefficient, it is necessary to divide the values of the pixels in $\mathcal{C}_i$ in two sequences x and y. However, the shape of $\mathcal{C}_i$ being arbitrary (as opposed to a square block of 16×16 pixels), it does not guarantee the validity of the neighborhood relationships used by Sutour *et al.* [22]. The division into two sequences x and y is therefore done randomly (by imposing that the two sequences are of the same length, potentially dropping one pixel if the total number of pixel values to be split is odd). This random splitting strategy, as opposed to the horizontal, vertical, diagonal, and anti-diagonal splitting applied to square blocks, is illustrated in Figure 1. In practice, the random division in

Fig. 5. Images *building*, *city*, *cobble*, *monument*, *shell* and *wall*.

sequences $x^{(k)}$ and $y^{(k)}$ is repeated K times in order to mitigate stochastic effects, and K p-values p_k of coefficients $\tau(x^{(k)}, y^{(k)})$ are calculated. The shape $\mathcal{C}_i$ is stated to be homogeneous if the 2^{nd} order statistic (the second smallest p-value) $p_{k(2)}$ exceeds the detection threshold α (in order to prevent the case where a test would be rejected only because of a particular arrangement of the division and not due to the inhomogeneity of the considered shape). The empircal mean $\hat{\mu}_i$ and variance $\hat{\sigma}_i^2$ of all homogeneous shapes further lead to the estimation of the NLF coefficients $\widehat{(a, b, c)}$ according to Equation (3). These different steps are illustrated in Figure 4.

4 Results

4.1 Experimental set-up

We evaluate our method on 6 images of dimensions 720×540 pixels shown in Figure 5. These are extracted from a high definition image database[1], for which the acquisition noise can be neglected. They were chosen to be as representative as possible in terms of morphological content, *i.e.*, to feature large homogeneous areas as well as small details and some textured regions. More precisely, we evaluate the robustness and the accuracy of the NLF estimated by our approach and by the method of Sutour *et al.* [22]. In a first step, we assess the robustness of the estimated NLF to the nature of the added noise. For that purpose, we add a non-mixed noise of varying intensity (setting to 0 the other two coefficients of the NLF), and we evaluate the ability of the NLF estimation method to practically estimate the right coefficient to be nonzero. If a Gaussian noise was added for instance, $(a, b) = (0, 0)$ in the corresponding NLF, and we thus check that it is

[1] http://www.gipsa-lab.grenoble-inp.fr/laurent.condat/imagebase.html

Table 1. Number of times (among the 6 trials) each NLF estimation method correctly retrieves the nature of the noise.

	building	*city*	*cobble*	*monument*	*shell*	*wall*
With blocks [22]	1/0/1	0/1/3	0/0/0	6/0/0	0/1/0	0/0/1
With shapes	6/4/4	4/3/5	4/2/6	0/5/4	2/3/6	0/0/6

also the case in the estimated NLF.
In a second step, we evaluate the estimation accuracy by artificially adding a mixed noise whose coefficients a, b and c (controling the NLF) are derived from a normal law $\mathcal{N}(0.01, 0.003)$ with mean 0.01 and standard deviation 0.003 (rounding to 0 negative coefficient). Note that the pixel values have been rescaled in the $[0:1]$ interval beforehand. In order to measure the estimation quality of NLF parameters, we calculate the mean relative error (MRE) between the reference $\mathrm{NLF}_{(a,b,c)}$ and the estimated $\mathrm{NLF}_{\widehat{(a,b,c)}}$ by

$$\mathrm{MRE}(\widehat{a,b,c}) = \frac{1}{|I|} \sum_{x_i \in I} \frac{|\mathrm{NLF}_{(a,b,c)}(x_i) - \mathrm{NLF}_{\widehat{(a,b,c)}}(x_i)|}{\mathrm{NLF}_{(a,b,c)}(x_i)}, \tag{6}$$

where I is a discretization of the pixel intensities interval $[0:1]$ in the image.
In any case, each noisy image is pre-filtered by a Gaussian filter with variance $\sigma = 1$ on which is built the ToS. The latter is simplified according to the Mumford-Shah functional, and we set the regularization parameter ν to be $200, 500, 1000, 2000$ and 5000. In the resulting simplified images, we consider only the shapes $\mathcal{C}_i$ whose size is greater than 250 pixels, on which the homogeneity test is conducted. This minimum size guarantees a reliable estimate of the Kendall coefficient of $\mathcal{C}_i$, as well as its empirical mean $\hat{\mu}_i$ and variance $\hat{\sigma}_i^2$ (note that in [22], the minimum size for a block b_i is $16 \times 16 = 256$ pixels). For each shape, the pixel values are randomly split $K = 10$ times in sequences $x^{(k)}$ and $y^{(k)}$, therefore leading to $K = 10$ Kendall tests. The second smallest p-value $p_{k(2)}$ is used to validate the homogeneity of the shape, namely whether it exceeds or not the detection threshold α fixed at $\alpha = 0.4$. This very restrictive detection threshold allows to really guarantee the homogeneity of all shapes detected as such.

4.2 Robustness of the estimated NLF

To evaluate the capacity of the NLF estimation method to retrieve the correct nature of the noise polluting the input image, we add a non-mixed noise of varying intensity, setting the other two parameters at 0 in the NLF. For each type of noise (multiplicative, Poisson, Gaussian), its associated parameter in the NLF (a, b and c, respectively) is set successively to 0.01, 0.015, 0.02, 0.025, 0.03 and 0.5 and we count how many times (among those 6 settings) the two NLF estimation methods practically estimate only the correct coefficient to be nonzero (note that we do not focus here on the accuracy of this estimated nonzero coefficient).

Table 2. Mean and standard deviation (in parenthesis) of the MRE between the reference NLF and the estimated NLF using square blocks and using shapes from the ToS. The given percentage corresponds to the number of times (with respect to the 20 draws) the use of shapes yields a NLF estimation with lower MRE than the use of square blocks.

	building	*city*	*cobble*	*monument*	*shell*	*wall*
With blocks [22]	0.0481 (0.0234)	0.0926 (0.1007)	0.8701 (0.7031)	0.2235 (0.0966)	0.1212 (0.0743)	0.1075 (0.1064)
With shapes	**0.0349** (0.0134) 65%	**0.0462** (0.0116) 85%	**0.0346** (0.0121) 100 %	**0.0552** (0.0201) 95%	**0.0385** (0.0124) 100%	**0.0513** (0.0102) 75%

Table 1 presents the obtained results, where a $x/y/z$ entry means that the multiplicative noise ($(b, c) = (0, 0)$) has been correctly identified x out of 6 times, the Poisson noise ($(a, c) = (0, 0)$) has been correctly identified y out of 6 times, and the Gaussian noise ($(a, b) = (0, 0)$) has been correctly identified z out of 6 times. Except for the multiplicative noise a on the image *monument*, our proposed NLF estimation method consistently obtains better results than the NLF estimated by square blocks. Note also that, in general, the estimation of a Gaussian noise seems much easier than for a multiplicative noise or Poisson noise, for which the L^1 minimization seems in general not to succeed nulling the c coefficient (corresponding to the offset).

4.3 Accuracy of the estimated NLF

To assess the accuracy of the estimated NLF coefficients, we add a mixed noise whose parameters a, b and c are drawn from a normal law $\mathcal{N}(0.01, 0.003)$ with mean 0.01 and standard deviation 0.003. We then compute the MRE between the true parameters (a, b, c) and the ones $(\widehat{a, b, c})$ that have been estimated using square blocks and shapes extracted from the ToS. We repeat this experiment 20 times for each image, and report in Table 2 the overall mean and standard deviation of the obtained MRE for both methods, as well as the percentage of times (with respect to the 20 draws) the NLF estimation based on shapes yields a lower (hence, better) MRE than its square blocks counterpart.
For the six studied images, the estimated NLF using shapes from the ToS consistently outperforms the NLF estimated with square blocks in terms of mean MRE, and with lower standard deviation. In the tighter case (being the *building* image), the proposed method still provides better results than the one of Sutour *et al.* [22] 13 times out of the 20 different draw (65%). This confirms sfrom a quantitative standpoint that the use of shapes adapted to the image content yields a more reliable and more robust estimation of the NLF.
To get a qualitative insight of this conclusion, Figure 6 presents the square blocks and shapes detected as homogeneous for the *building* image polluted with a mixed noise of coefficients $(a, b, c) = (1.22.10^{-2}, 0.82.10^{-2}, 0.82.10^{-2})$, as well as the estimated NLF coefficients in each case. In the first case, 104

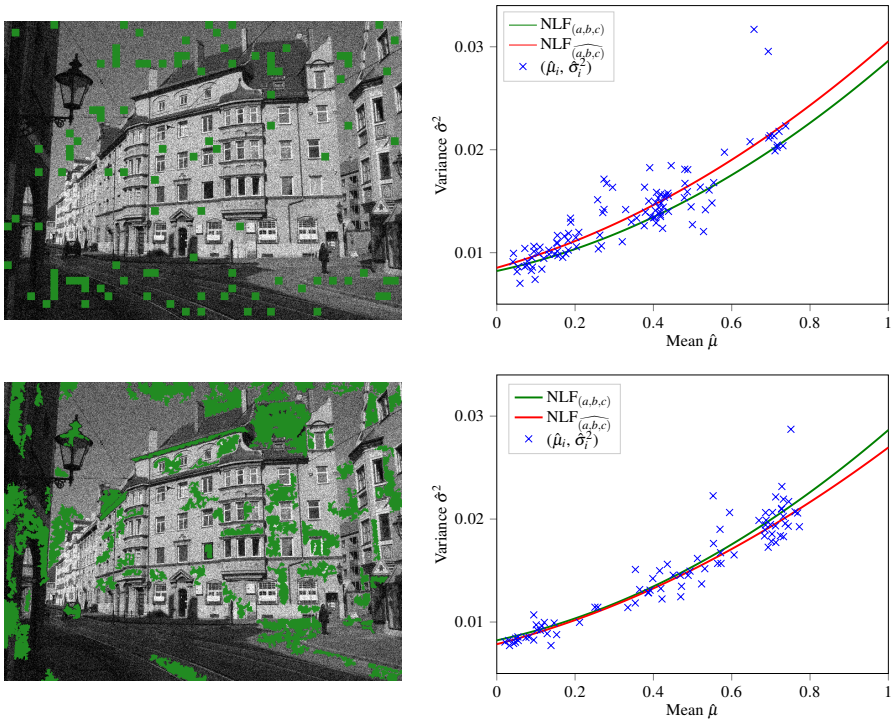

Fig. 6. First row: *blocks* detected as homogeneous for a mixed noise added to the *building* image (left) and estimated NLF compared to the reference NLF (right). Second row: *shapes* detected as homogeneous for the same noise (left), and corresponding estimated NLF compared to the reference NLF (right).

square blocks were detected as homogeneous, leading to the coefficient estimates $(\widehat{a,b,c}) = (1.12.10^{-2}, 1.07.10^{-2}, 0.85.10^{-2})$ and a MRE of $7.56.10^{-2}$. In the second case, 81 homogeneous shapes were detected from the various Mumford-Shah simplifications of the ToS constructed on the *building* image, leading to $(\widehat{a,b,c}) = (0.93.10^{-2}, 0.98.10^{-2}, 0.78.10^{-2})$ for the NLF coefficient estimation and a MRE of $2.96.10^{-2}$. While the number of homogeneous regions used to estimate the NLF coefficients is of the same order of magnitude for both competing methods (although being smaller when using the ToS), the size of the detected homogeneous regions drastically differs. In [22], square blocks are limited to $16 \times 16 = 256$ pixels since the image content is unknown *a priori* and cannot be assumed to comprise large homogeneous areas. Since this limitation vanishes with the use of regions adapting to the image content, shapes of significantly larger sizes are detected as homogeneous. This lead to a more precise evaluation of their empirical mean $\hat{\mu}_i$ and variance $\hat{\sigma}_i^2$ since more samples are used, hence a less vertically dispersed scatterplot $\{(\hat{\mu}_i, \hat{\sigma}_i^2)\}$, as it can be seen on Figure 6, resulting in a more accurate and more robust estimation of the NLF coefficients with fewer regions.

5 Conclusion

In this article, we have presented an extension of the method of Sutour *et al.* [22] to estimate the NLF of some noisy images. The key idea is to replace the search for homogeneous square blocks by that of homogeneous shapes, extracted from a tree of shapes simplified using the Mumford-Shah functional. As a consequence, the computation of the noise statistics is performed on regions adapted to the morphological content of the image, making the NLF estimation more robust and more accurate. Eventually, we are able to better identify the nature and characteristics of the noise polluting the image. A major perspective of our work is to adapt the NLF estimation to color images, since a definition of the tree of shapes already exists for multivariate images [4].

References

1. Ballester, C., Caselles, V., Monasse, P.: The tree of shapes of an image. ESAIM: Control, Optimisation and Calculus of Variations **9**, 1–18 (2003)
2. Beaurepaire, L., Chehdi, K., Vozel, B.: Identification of the nature of noise and estimation of its statistical parameters by analysis of local histograms. In: 1997 IEEE International Conference on Acoustics, Speech, and Signal Processing. vol. 4, pp. 2805–2808. IEEE (1997)
3. Buades, A., Coll, B., Morel, J.M.: A review of image denoising algorithms, with a new one. Multiscale Modeling & Simulation **4**(2), 490–530 (2005)
4. Carlinet, E., Géraud, T.: MToS: A tree of shapes for multivariate images. IEEE Transactions on Image Processing **24**(12), 5330–5342 (2015)
5. Carlinet, E., Géraud, T., Crozet, S.: The tree of shapes turned into a max-tree: A simple and efficient linear algorithm. In: Proceedings of the 24th IEEE International Conference on Image Processing (ICIP). pp. 1488–1492. Athens, Greece (2018)
6. Chambolle, A., Pock, T.: A first-order primal-dual algorithm for convex problems with applications to imaging. Journal of mathematical imaging and vision **40**(1), 120–145 (2011)
7. Crozet, S., Géraud, T.: A first parallel algorithm to compute the morphological tree of shapes of nD images. In: Proceedings of the 21st IEEE International Conference on Image Processing (ICIP). pp. 2933–2937. Paris, France (2014)
8. Dabov, K., Foi, A., Katkovnik, V., Egiazarian, K.: BM3D image denoising with shape-adaptive principal component analysis. In: SPARS'09-Signal Processing with Adaptive Sparse Structured Representations (2009)
9. Deledalle, C.A., Duval, V., Salmon, J.: Non-local methods with shape-adaptive patches (NLM-SAP). Journal of Mathematical Imaging and Vision **43**(2), 103–120 (2012)
10. Donoho, D.L.: De-noising by soft-thresholding. IEEE transactions on information theory **41**(3), 613–627 (1995)
11. Droske, M., Rumpf, M.: Multiscale joint segmentation and registration of image morphology. IEEE transactions on pattern analysis and machine intelligence **29**(12), 2181–2194 (2007)
12. Freeman, W.T., Jones, T.R., Pasztor, E.C.: Example-based super-resolution. IEEE Computer graphics and Applications (2), 56–65 (2002)

13. Géraud, T., Carlinet, E., Crozet, S., Najman, L.: A quasi-linear algorithm to compute the tree of shapes of nD images. In: Mathematical Morphology and Its Application to Signal and Image Processing – Proceedings of the 11th International Symposium on Mathematical Morphology (ISMM). Lecture Notes in Computer Science, vol. 7883, pp. 98–110. Springer (2013)
14. Kendall, M.G.: The Treatment of Ties in Ranking Problems. Biometrika **33**(3), 239–251 (1945), http://www.jstor.org/stable/2332303
15. Kendall, M.G.: A new measure of rank correlation. Biometrika **30**(1/2), 81–93 (1938)
16. Liu, C., Freeman, W.T., Szeliski, R., Kang, S.B.: Noise estimation from a single image. In: Computer Vision and Pattern Recognition, 2006 IEEE Computer Society Conference on. vol. 1, pp. 901–908. IEEE (2006)
17. Liu, X., Tanaka, M., Okutomi, M.: Single-image noise level estimation for blind denoising. IEEE transactions on image processing **22**(12), 5226–5237 (2013)
18. Mäkitalo, M., Foi, A.: Noise parameter mismatch in variance stabilization, with an application to poisson–gaussian noise estimation. IEEE Transactions on Image Processing **23**(12), 5348–5359 (2014)
19. Monasse, P., Guichard, F.: Fast computation of a contrast-invariant image representation. IEEE Transactions on Image Processing **9**(5), 860–872 (2000)
20. Mumford, D., Shah, J.: Optimal approximations by piecewise smooth functions and associated variational problems. Communications on pure and applied mathematics **42**(5), 577–685 (1989)
21. Pyatykh, S., Hesser, J.: Image sensor noise parameter estimation by variance stabilization and normality assessment. IEEE Transactions on Image Processing **23**(9), 3990–3998 (2014)
22. Sutour, C., Deledalle, C.A., Aujol, J.F.: Estimation of the noise level function based on a nonparametric detection of homogeneous image regions. SIAM Journal on Imaging Sciences **8**(4), 2622–2661 (2015)
23. Walker, J.S.: Combined image compressor and denoiser based on tree-adapted wavelet shrinkage. Optical Engineering **41**(7), 1520–1528 (2002)
24. Xu, Y., Géraud, T., Najman, L.: Hierarchical image simplification and segmentation based on Mumford–Shah-salient level line selection. Pattern Recognition Letters **83**, 278–286 (2016)